International Journal of Mining and Geo-Engineering

IJMGE

IJMGE 51-1 (2017) 63–69

DOI: 10.22059/ijmge.2016.218204.594633

A Numerical Analysis on the Performance of Counterweight Balance on the Stability of Undercut Slopes

Mohammad Hossein Khosravi[a*], Hassan Sarfaraz[a], Mahmoud Esmailvandi[a], Thirapong Pipatpongsa[b]

[a] *School of Mining, College of Engineering, University of Tehran, Iran*

[b] *Department of Urban Management, Kyoto University, Japan*

Article History:

Received 19 October 2016,

Revised 10 December 2016,

Accepted 30 December 2016.

ABSTRACT

Determining the maximum stable undercut span is an important parameter in undercut slopes design. The maximum stable undercut span is a function of slope geometry, the strength parameters of the slope material, condition of discontinuities, underground water condition, etc. However, the desired production capacity and therefore the size of excavating equipment will sometimes ask for a wider undercut span. The influence of arching phenomenon in geo-material on the stability of undercut slopes is investigated earlier. It is believed that due to the arching effect, some load transfer from the undercut area into stationary remaining side toes leads to a more stable slope. However, the transferred load may result in ploughing failure of side toes. One technique for preventing the ploughing failure is application of counterweight balance on side toes. In this study, the influence of counterweight size on the stability of the undercut slopes was investigated through a series of numerical model tests using FLAC3D software. It was concluded that there was a meaningful relationship between the counterweight balance size and the maximum stable undercut span where increasing a counterweight size resulted in a wider stable span. Finally, the numerical results were compared with pre-conducted physical modeling test and a nonlinear relationship was proposed between the counterweight size and the maximum stable undercut span.

Keywords : *Numerical Modeling, Arching Effect, Undercut Slopes, Counterweight Balance.*

1. Introduction

The slopes stability is a major problem in geotechnical engineering where a slope failure sometimes may cause catastrophic damages and casualties. The term "undercut slopes" in this study will refer to those slopes in surface mining where the process of excavation is under operation in front of them. Determining the optimum undercut span is an important issue in undercut slopes, where on one hand the span is limited to a maximum size depending on the strength properties of slope material, and on the other hand, it is limited to a minimum size depending on the desired production capacity and the size of mining equipment [1].

In calculation of the undercut span, the phenomenon of arch action plays an important role. This phenomenon in geo-material was introduced by Terzaghi (1936), as load transferring from a yielding portion of the geo-material to its stable portions [2]. Many researchers investigated the soil arch action in different fields and investigated this phenomenon theoretically, numerically and physically [3-7].

Wang & Yen (1973) were among pioneers who investigated arching effect in slopes [8]. Bosscher and Gray (1986) studied this phenomenon for sandy slopes through physical modeling [6]. Hassiotis et al. (1997) tried to find a designing method for pile stabilized slopes considering arch action [9]. Later, other researchers tried to investigate arch action in pile stabilized slopes such as Chen & Martin (2002), Hosseinian & Cheraghi (2013), Zhao & Zhai (2014) and Li et al. (2015). [10-13].

Pipatpongsa et al. (2009) investigated the stability of undercut slopes in Mea Moh open pit Lignite mine in Lampang city of Thailand. They suggested an excavation technique based on arching action and cut and fill technique to solve stability problems. Excavation by Sequence of this method could provide the expected stability without any special supporting equipment [14].

Khosravi et al. (2009, 2011) conducted some physical model tests using humid sand to examine the possible failure modes in undercut slopes. They reported five different slope failure modes depending on the slope geometry and loading conditions [15, 16].

Later a series of centrifugal physical model tests were conducted by Khosravi et al. (2016) using the Mark III beam centrifuge of the Tokyo Institute of Technology. In that study, the earth pressure and the movement distribution were recorded by pressure cells and using particle image velocimetry (PIV), respectively at each excavation step. The results showed that arch action also accrued to undercut slopes under high gravitational acceleration confirming that the arch action is a size independent phenomenon [17].

The unstable undercut slopes can be stabilized by means of different reinforcing techniques such as anchoring, counterweight balance, etc. The use of some types of shear pins for stabilizing undercut slopes are studied physically and numerically by Ouch et al. (2016, 2017) and Ukritchon et al. (2017) [18-20]. The influence of counterweight balance on the stability of undercut slopes then was studied through some physical model tests under 1-g condition and was applied to Mae Moh open-pit mine as a case study [21]. It was confirmed that as the width of the counterweight area increased, the pillars of the model become stronger leading to a more stable undercut slope. Therefore, the excavated area could become wider compared to the slopes without counterweight balance [22]. However, due to limitations and difficulties in physical modeling, the study of counterweight balance was done

* Corresponding author. Tel.: (+98) 9128409645; *E-mail address:* mh.khosravi@ut.ac.ir (M.H.Khosravi).

through a limited number of model tests. In order to develop the previous study, a series of numerical modeling tests were done using finite difference method, FLAC 3D software. The relationship between the counterweight balance size and the maximum stable undercut span is confirmed by comparison between the results of numerical and physical models.

2. Introduction Modeling Matherial Characteristics

As the numerical investigation in this study was established to complete the results of the pre-conducted physical modeling study [22], the material properties were selected the same with those used in physical models. The material properties in the physical and numerical models are listed in Table 1 and Table 2, respectively. Note that the cohesion values measured by experimental tests ranges from 0.36 kPa to 8 kPa for used modelling material. In order to select an appropriate cohesion value for numerical models, the model was repeated without counterweight with cohesion values ranging from 0.36 kPa to find the maximum undercut span equivalent to that observed in physical model. The cohesion value of 0.95 kPa was obtained as the appropriate value and was used for numerical models.

Table 1. Material properties of moist silica sand No. 6 used in physical models [1, 22, and 23]

Material properties (Physical Model)	Value
Bulk density (ρ)	1395 kg/m^3
Specific density (G_s)	2.650
Maximum void ratio (e_{max})	1.132
Minimum void ratio (e_{min})	0.711
Water content (ω)	10 %
Internal friction angle (φ)	41.5°
Interface friction angle on Teflon sheet (δ)	18.5°
Apparent cohesion (c)*	0.36-8.00 kPa
Apparent adhesion on Teflon sheet (c_t)	0.10 kPa
*Different values of cohesion are reported for this soil [1, 22, 23].	

Table 1. Material properties used in numerical models

Material properties (Numerical Model)	Value
Bulk density (ρ)	1395 kg/m^3
Bulk Modulus (K)	2.67×10^3 kPa
Shear Modulus (G)	1.67×10^3 kPa
Normal interface stiffness (k_n)	1×10^6 kPa/m
Shear interface stiffness (k_s)	1×10^6 kPa/m
Internal friction angle (φ)	41.5°
Interface friction angle (δ)	18.5°
Cohesion (c)	0.95 kPa
Adhesion (c_t)	0.10 kPa

3. Numerical Modelling

3.1. Model Geometry and data recording

The numerical model is illustrated schematically in Fig. 1. As indicated in this figure, the model consists of cubic elements with the size of 0.02 m. Choosing the size of element larger than this amount reduced the accuracy of modeling, and the element size smaller than this increased the calculation time enormously. The geometry of the numerical model was selected exactly similar to that of a previous physical modeling study. A photo of the physical model is shown in Fig. 2 for comparison. The model was generally composed of two parts: the base part with the dimensions of W=1.0 m by LT=0.4 m and the slope part with the dimensions of W=1.0 m by LS=0.6 m. The slope part had an inclination angle of α=50o and the thickness of the model was H=0.06 m in both slope and base parts. The counterweights were simulated by using the same material used in simulation of the whole model. The influence of the counterweight on the stability of the slope was studied by simulating models with different sizes of the counterweights.

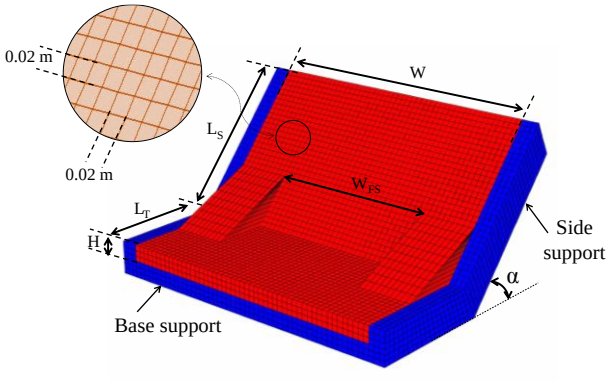

Fig. 1. Schematic of numerical model

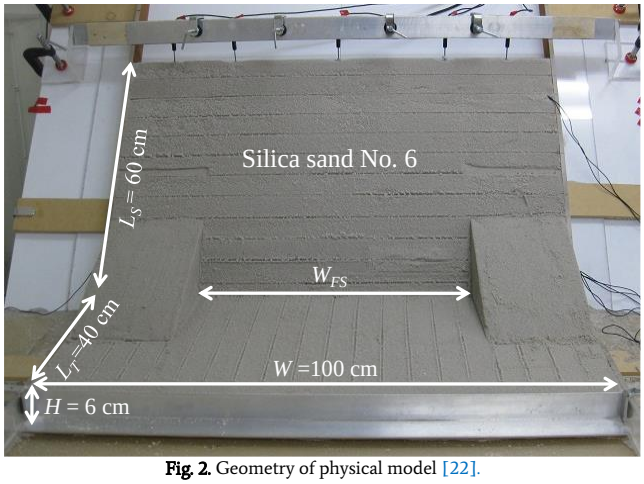

Fig. 2. Geometry of physical model [22].

In order to make the modeling results comparable with the pre-conducted physical models, the location of the pressure cells used in physical models was selected as earth pressure control points in the numerical models.

The model was left to balance after preparation and before starting the undercut process. When the maximum unbalanced force recorded in the model was reduced to zero, as shown in Fig. 3, then the model was ready for undercutting.

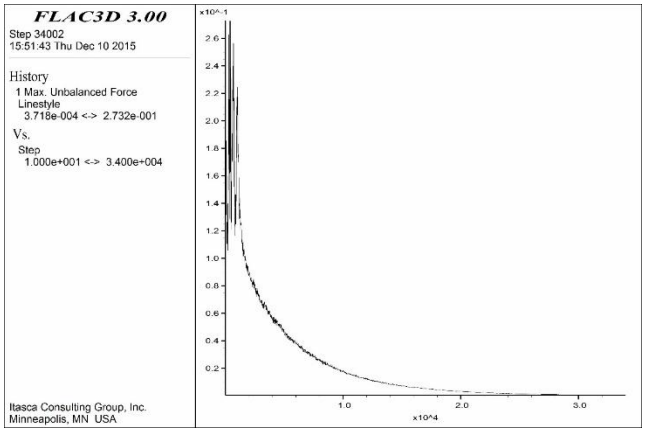

Fig. 3. Change in maximum unbalanced force before undercut process

3.2. Undercut process

The Mohr-Coulomb yield criterion was used in this study. According to this criterion, the model is considered to be in equilibrium as long as the

maximum unbalanced force is ignorable compared to the total applied forces in the problem. If the unbalanced force approaches a constant nonzero value, this indicates that failure and plastic flow are occurring within the model [24].

The undercut process followed the approach done in physical modeling. This process is explained in details for model test 5 in this section. The process starts by removing a central slice, 4 cm in width, from the base part of the model as shown in Figure 4(a). The model was allocated some time to balance again and therefore the maximum unbalanced force was reduced to zero (Fig. 4(b)). Then the undercut span was extended symmetrically with steps of 4 cm (2 cm leftward and 2 cm rightward) and rebalanced until the model failed. The existence of unbalanced force in the model indicates the model failure. For the model test 5 the maximum stable undercut span was 36 cm which reached at the 9th undercut step and the failure occurred after the 10th undercut step. The geometry of the model and the record of the maximum unbalanced force in the model are shown in Fig. 5.

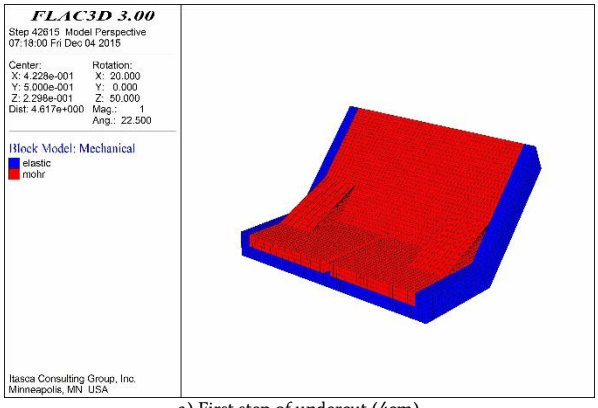

a) First step of undercut (4cm)

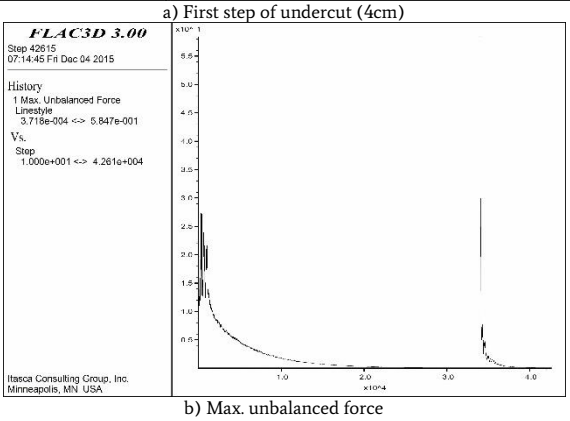

b) Max. unbalanced force

Fig. 4. First step of undercut process for model test 5

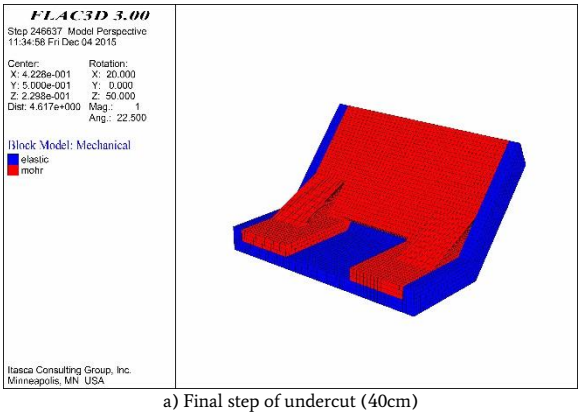

a) Final step of undercut (40cm)

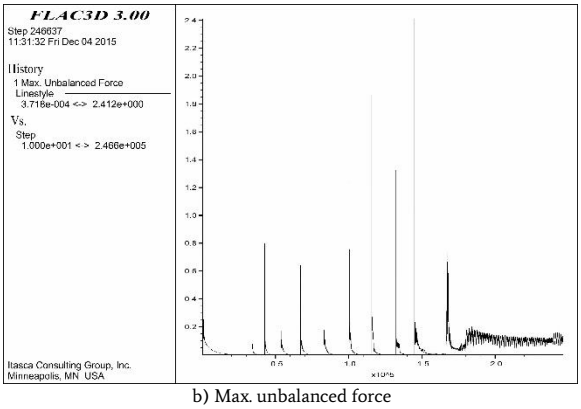

b) Max. unbalanced force

Figure 5. Final step of undercut process for model test 5

Records of maximum unbalanced forces during undercut process in all the numerical model tests are shown in Fig. 6.

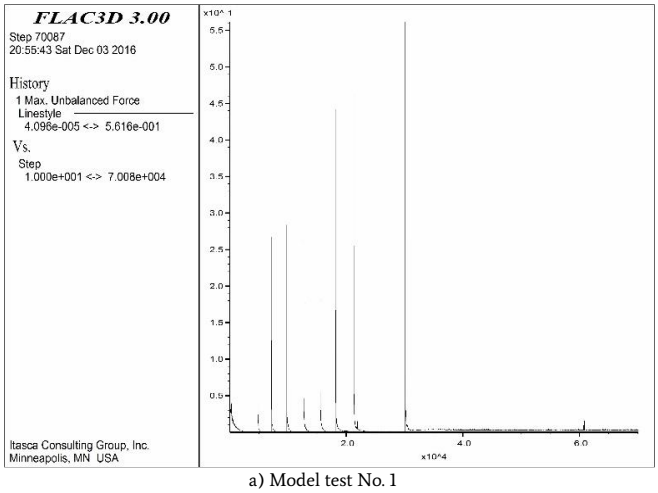

a) Model test No. 1

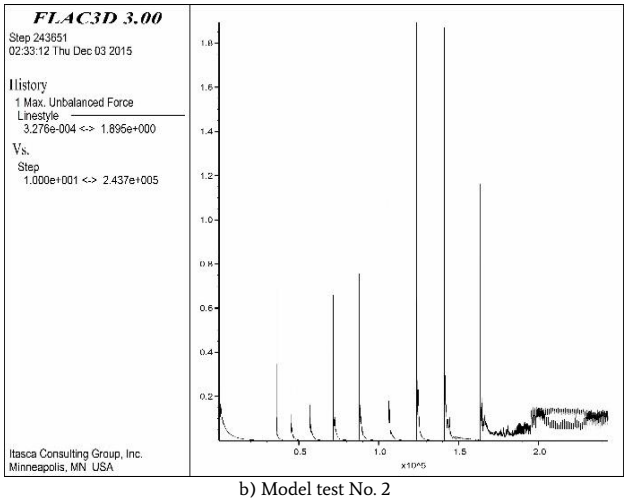

b) Model test No. 2

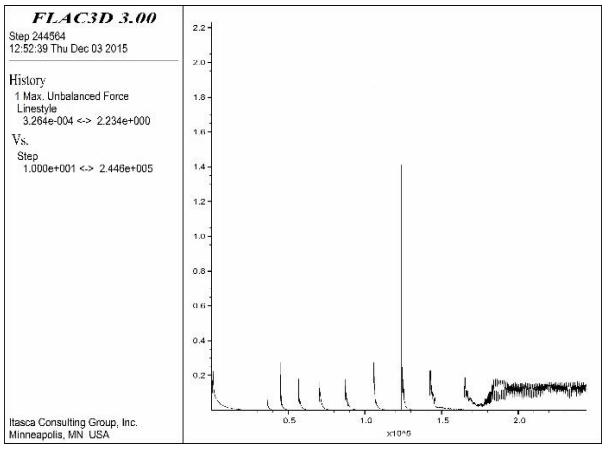

c) Model test No. 3

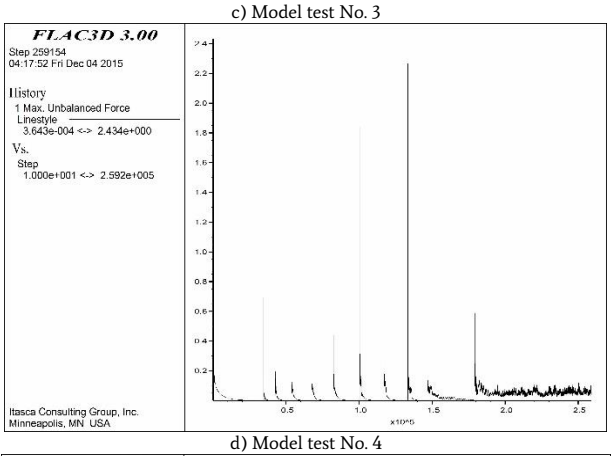

d) Model test No. 4

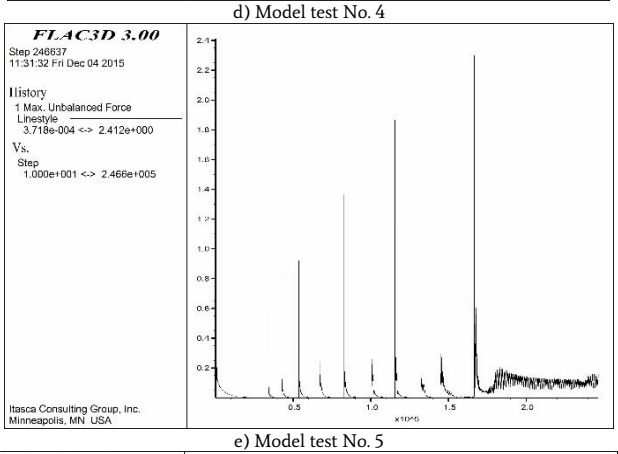

e) Model test No. 5

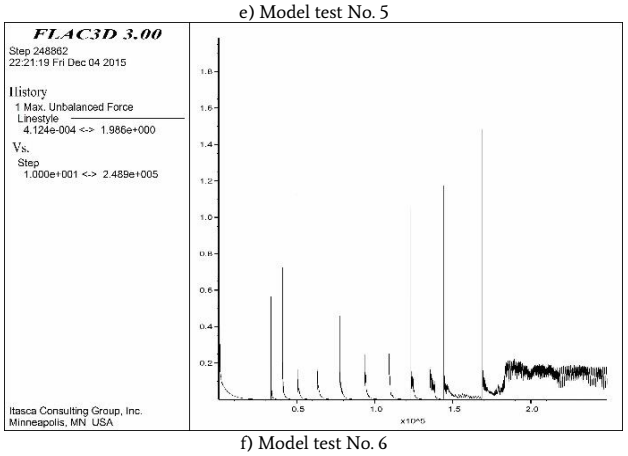

f) Model test No. 6

Fig. 6. Records of maximum unbalanced forces during undercut process in numerical model tests

4. Numerical Results and discussion

4.1. Failure modes

Contours of failure modes occurred in numerical model No. 5 is shown in Fig. 7(a). As shown, it is obvious that shear cracks initiated from the corner of the undercut area. The other parts of the model are mostly under tension stresses. These results are consistent with that of the physical models. The crack initiation captured by means of a high speed camera in the physical model No. 5 is shown in Fig. 7(b) for comparison.

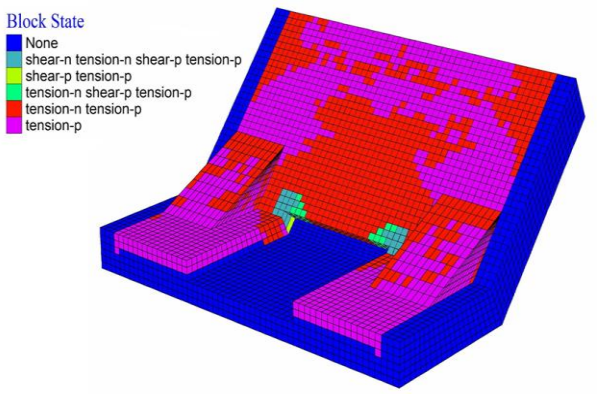

a) Numerical model (B_{MS}=36 cm)

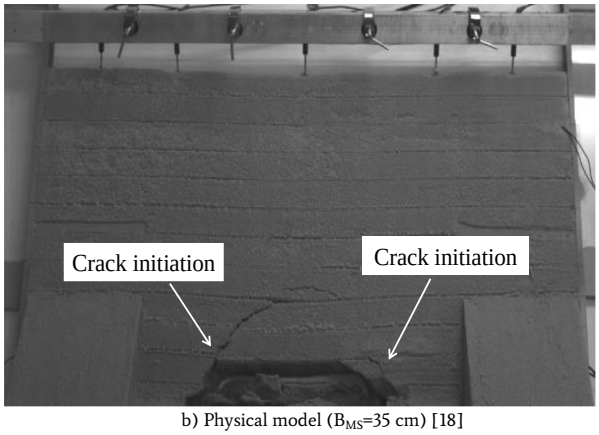

b) Physical model (B_{MS}=35 cm) [18]

Fig. 7. The crack initiation in the model No. 5

Contours of shear stress in the numerical slope model No. 5 are shown in Fig. 8. It is clearly seen in this figure that the maximum shear stress appeared in the area between the slope part immediately above the undercut area and the counterweights. Actually the role of the counterweight balance in increasing the stability of the undercut slopes can be explained by the location of the maximum shear stress and arching effect. By undercutting the slope, the part of the slope immediately above the undercut area lose its support and tend to slip down along the sloping plate. This movement of the soil mass activates the shear stress between the moving part and the adjacent stationary parts of the slope. According to the arching effect, the shear stress helps the load to transfer from the moving part and the adjacent stationary parts. As a result, the weight of the moving soil mass will be supported partially by the counterweights and therefore the failure of the slope will be delayed compared to the slope without counterweights.

Unfortunately, in conducting the physical models, it was impossible to measure the shear stress in the model. However, the contours of shear strain were obtained from the models by means of particle image velocimetry (PIV). PIV is a recently developed nondestructive image processing technique, which uses consecutive digital images captured from the surface of the model to record the model deformation [25].

Contours of shear strain in the physical slope model No. 5 are shown in Fig. 9. These results are somehow comparable with those of Fig. 8 where both shear stress and shear strain are maximized in the same area of the models.

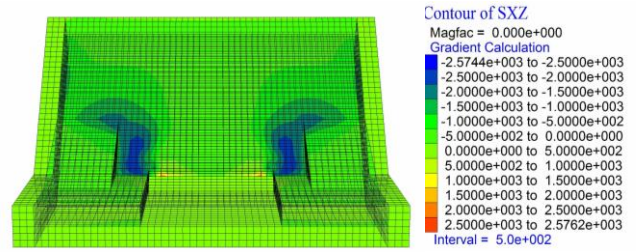

Fig. 8. Contours of shear stress in the numerical model No. 5

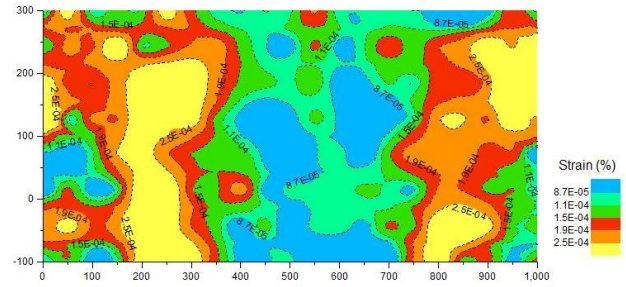

Fig. 9. Contours of shear strain in the physical model No. 5

4.2. Stress redistribution and arching effect

The location of embedded pressure cells in the physical models is schematically shown in Figure 10. As mentioned before the location of the control points in the numerical models were selected exactly at the same location of pressure cells used in the physical models where the depth of embedment was half of slope thickness. Furthermore, the directions of the recorded earth pressures were consistent in both numerical and physical models.

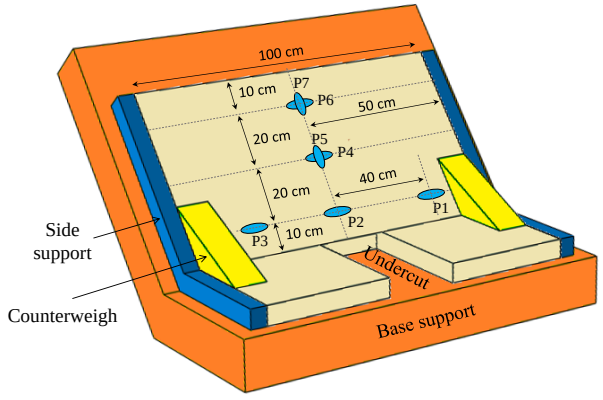

Fig. 10. Instrumentation of the model

Plots of the earth pressure recorded in the control points inside the numerical models are plotted as a function of the undercut span in Fig. 11. Where the undercut span (B) and the measured earth pressure (P) are normalized by the slope width (W) and ρgH (ρ : bulk density of the sand, g: earth's gravity; H: thickness of the model), respectively. Due to the symmetrical condition, variations of earth pressure with respective to undercut span for P1 and P3 are exactly the same.

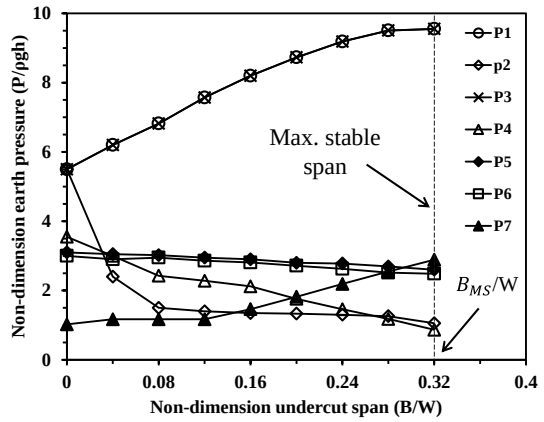

a) Model test No. 1 (CW=0cm)

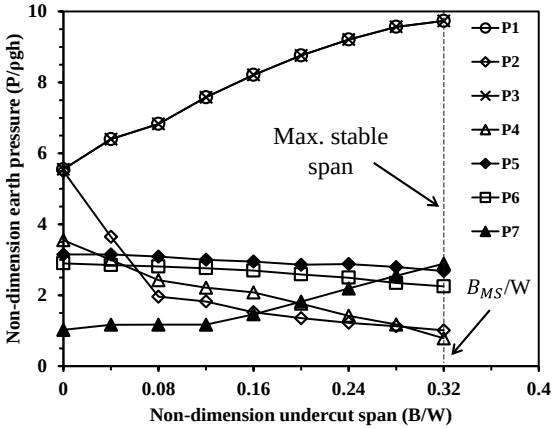

b) Model test No. 2 (CW=6cm)

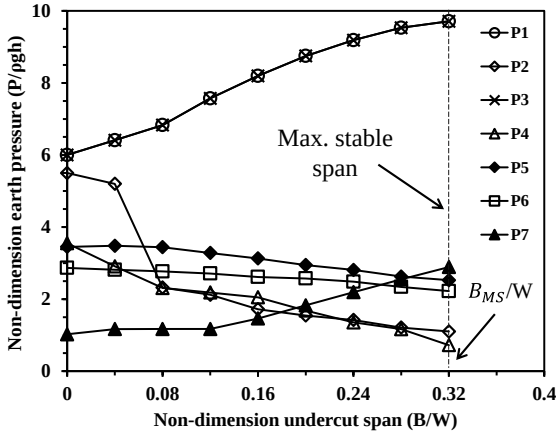

c) Model test No. 3 (CW=10cm)

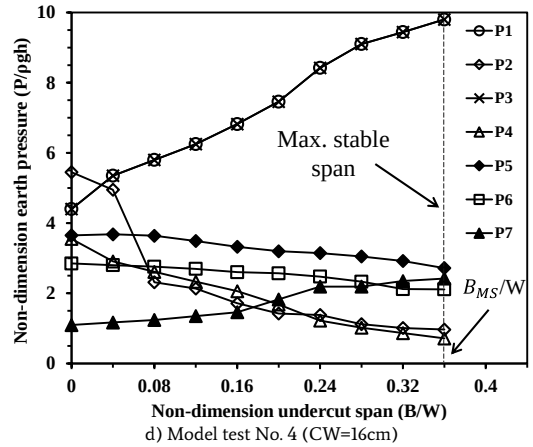

d) Model test No. 4 (CW=16cm)

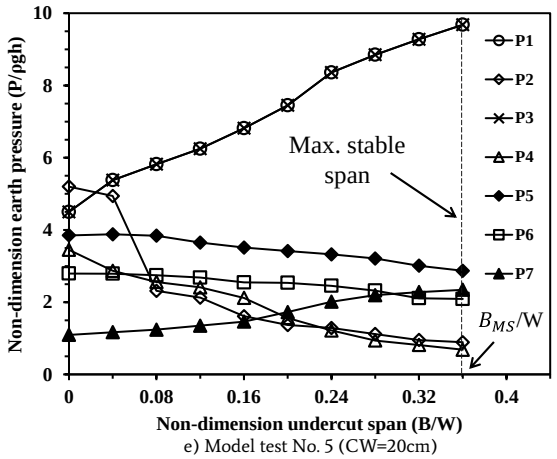

e) Model test No. 5 (CW=20cm)

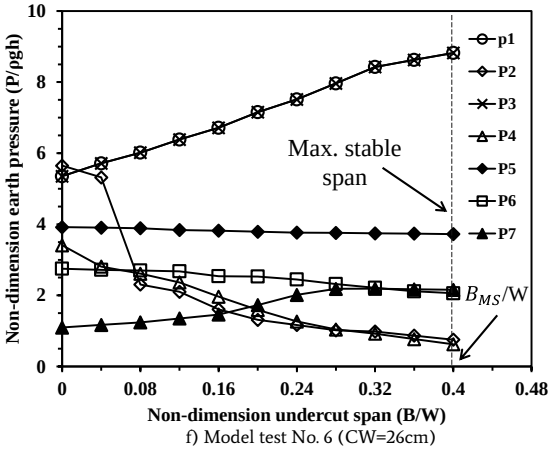

f) Model test No. 6 (CW=26cm)

Fig. 11. Records of earth pressure vs. undercut span in numerical models

Plots of the earth pressure recorded by pressure cells in the physical model test No. 5 are shown in Fig. 12 for comparison.

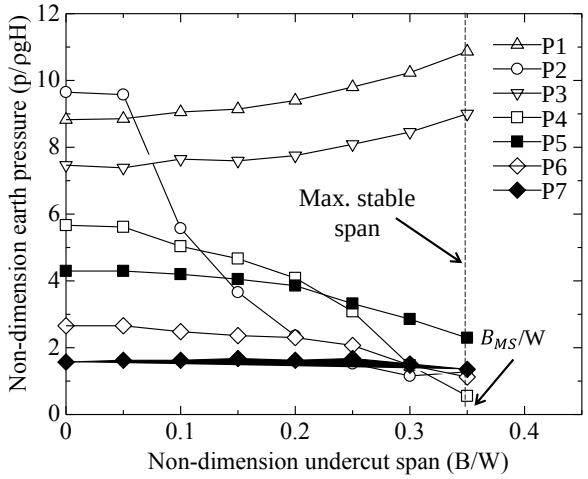

Fig. 12. Records of earth pressure vs. undercut span in physical model test No. 5 [22]

Considering the pressure cells and control points at lower level in the slope (i.e. P1, P2 and P3), as the undercut span increase, the earth pressure decreases in the central part (P2) while increases in sides (P1 and P3). This earth pressure redistribution is an obvious evidence of the arching effect showing a load transfer process from central loosing part to adjacent stationary parts of the model. Furthermore, looking at the pressure values recorded by the uppermost pair of pressure cells and control points (P6 and P7), it can be seen that before the undercut process begins, the stress condition is active (P6>P7) while by expanding the undercut span the stress condition changes gradually to passive (P6<P7). This stress switch from active to passive is again an evidence of arching effect where stress arches appeared in the undercut slope.

The above mentioned phenomena and trends of stress redistributions were observed in both numerical and physical model tests consistently. However, there was an inconsistency in the initial pressure values recorded in numerical and physical models. The inconsistency is related to the difference in model preparation.

4.3. Formulation of the maximum undercut span

The total number of six numerical model tests were conducted with different counterweight sizes as listed in Table 3. The results of three pre-conducted physical model tests are also listed in this table for comparison.

Table 3. Results of numerical and physical modelling

Model No.	Counterweight width (m)	Type of modeling	Max. stable undercut span (m)
1	0	Numerical	0.32
		Physical [18]	0.30
2	0.06	Numerical	0.32
3	0.10	Numerical	0.32
4	0.16	Numerical	0.36
5	0.20	Numerical	0.36
		Physical [18]	0.35
6	0.26	Numerical	0.40
7	0.30	Physical [18]	0.40

The normalized maximum stable undercut span (B_{MS}/W_{FS}) is plotted as a function of the normalized free span (W_{FS}/W) in Fig. 13. The free span refers to the span between two counterweights as indicated in Fig. 1 and Fig. 2. As seen in Fig. 13, the maximum stable undercut span increases as the free span decreases. In other words, an increase in the size of the counterweights results in approaching to a wider stable undercut span. These results are in agreement with the previous results of the physical modeling study [22]. The technique of counterweight balance can be utilized to increase final stable undercut span, and therefore, to increase the stability of undercut slopes.

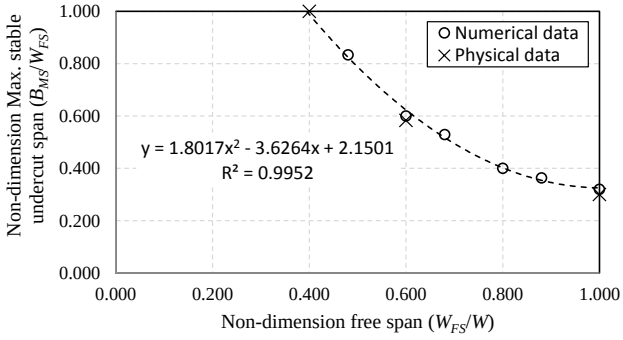

Fig. 13. Maximum stable undercut span vs. free span

5. Conclusion

The influence of counterweigh balance on the stability of undercut slopes was investigated numerically in this study. FLAC 3D as a finite

difference software was utilized for this investigation. A set of numerical model tests were done with a variety of counterweight balance sizes. The results of this study confirmed the development of arching phenomena in the undercut slopes, where the Mohr-coulomb yield criterion was applied to the modeling material. It can be concluded that for geo-materials modeled in this study, under a symmetrical cutting process, counterweight balance can be considered as a useful technique in increasing the stability of undercut slopes. These results are in good agreement with the results of a pre-conducted series of physical model tests. The technique of counterweight balance can be useful in stabilizing the undercut slopes such as those in surface coal mining under special conditions. Under application of this technique, the equipment operational space can be increased while the risk of slope failure during operation decreased.

References

[1] Khosravi, M.H. (2012). Arching effect in geomaterials with applications to retaining walls and undercut slopes. Ph.D. dissertation, Tokyo Institute of Technology, Tokyo, Japan.

[2] Terzaghi, K. (1936). Stress distribution in dry and saturated sand above a yielding trap-door. Proc., 1st Int. Conf. Soil Mechanics Foundation Engineering, Harvard Univ., Cambridge, MA, 307–311.

[3] Janssen, H.A. (1895), Versuche über Getreidedruck in Silozellen (Texts on grain pressure in silos), Zeitschr. d. Vereines deutscher Ingenieure 39, 1045-1049.

[4] Spangler, M.G. (1964), Protection of Underground Structures by Arch Action Associated with the Imper-fect Ditch Method of Construction, Proceedings of the Symposium on Soil-Structure Interaction University of Arizona, Tucson, Arizona, pp. 531-546.

[5] Handy, R.L. (1985), The arch in soil arching. ASCE Journal of Geotechnical Engineering, Vol. 111, No. 3, pp. 302-318.

[6] Bosscher, p.J. and Gray, D.H. (1986), Soil arching in sandy slopes methods. Journal of Geotechnical Engineering, 112 (6): 626-645.

[7] Khosravi, M.H., Pipatpongsa, T., Takemura, J. (2013), Experimental analysis of earth pressure against rigid retaining walls under translation mode, Géotechnique 63, No.12, 1020-1028.

[8] Wang, W.L., Yen, B.C. (1974), Soil arching in slopes, Journal of the Geotechnical Engineering Division - ASCE 100, No.GT1, 61-78.

[9] Hassiotis, S., Chameau, J.L., Gunaratne M. Design method for stabilization of slopes with piles. J Geotech Geoenviron Eng 1997; 123(4):314–23.

[10] C.-Y. Chen, G.R. Martin, (2002), Soil-structure interaction for landslide Stabilizing piles, Computers and Geotechnics 29 (2002) 363–386.

[11] Hosseinian, S., Seifabad, M.C., Optimization the Distance between Piles in Supporting Structure Using Soil Arching Effect, (2013), Journal of Civil Engineering and Urbanism Volume 3, Issue 6: 386-391.

[12] Zhao Bo, Zhai Yong-chao, (2014), Analysis of soil arching effect with different cross-section antislide pile, Journal of Engineering Research and Applications ISSN: 2248-9622, Vol. 4, Issue 12 (Part 4), pp.05-10.

[13] Li, C., Wu, J., Tang, H., Wang, J., Chen, F., Liang, D., (2015), A novel optimal plane arrangement of stabilizing piles based on soil arching effect and stability limit for 3D colluvial landslides.

[14] Pipatpongsa, T., Khosravi, M.H., Doncommul, P., and Mavong, N. (2009). Excavation problems in Mae Moh lignite open-pit mine of Thailand. Proc., Geo-Kanto, Tochigi, 459-464.

[15] Khosravi, K.H., Pipatpongsa, P. Leelasukseree, C. Wattanachai, P. Failure mechanisms in arched excavation of earth slope using model test. (2009)

[16] Khosravi, M.H., Pipatpongsa, T., Takahashi, A., and Takemura, J. (2011). Arch action over an excavated pit on a stable scarp investigated by physical model tests. Soils and Foundations, 51(4), 723-735.

[17] Khosravi, M.H., Pipatpongsa, T., Takemura, J., and Amini, M. (2016). In-flight Excavation of Slopes with Potential Failure Planes. Journal of Geotechnical and Geoenvironmental Engineering, 142(5), DOI 10.1061/(ASCE)GT.1943-5606.0001439.

[18] Ouch, R., Ukritchon, B., Pipatpongsa, T. and Khosravi, M. H. (2016). Experimental investigations of shear pin arrangement on soil slope resting on low interface friction plane, Maejo International Journal of Science and Technology, 10(03):313-329.

[19] Ouch, R., Ukritchon, B., Pipatpongsa, T. and Khosravi, M. H. (2017). Finite element analyses of the stability of a soil block reinforced by shear pins, Geomechanics and Engineering, 12(6). Published online. https://doi.org/10.12989/gae.2017.12.6.000.

[20] Ukritchon, B., Ouch, R., Pipatpongsa, T. and Khosravi, M. H. (2017). Experimental studies of floor slip tests on soil blocks reinforced by brittle shear pins, International Journal of Geotechnical Engineering, Published online. http://dx.doi.org/10.1080/19386362.2017.1314126.

[21] Pipatpongsa, T., Khosravi, M. H. and Takemura, J. (2013). Physical modeling of arch action in undercut slopes with actual engineering practice to Mae Moh open-pit mine of Thailand. Proceedings of the 18th International Conference on Soil Mechanics and Geotechnical Engineering (ICSMGE18), Paris, France, 943-946.

[22] Khosravi, M.H., Tang, T., Pipatpongsa, P., Takemura, J., and Doncommul, P. (2012). Performance of counterweight balance on stability of undercut slope evaluated by physical modeling. International Journal of Geotechnical Engineering (2012) 6: (193-205), OI 10.3328/IJGE.2012.06.02.193-205.

[23] Leelasukseree, C., Pipatpongsa, T., Khosravi, M.H., and Mavong, N. (2012). Stresses and a failure mode from physical and numerical models of undercut slope lying on inclined bedding plane, The 7th Asian Rock Mechanics Symposium, Seoul, Korea.

[24] Itasca. Group. Inc. (2007), FLAC3D Fast Lagrangian Analysis of Continua in 3 Dimension, Version 3.0, User' Manual.

[25] White, D. J., Randolph, M. & Thompson, B. (2005). An image based deformation measurement system for the geotechnical centrifuge. Int. J. Phys. Model. Geotech. 5, No. 3, 1–12.